Luminescent $Pt^{II}-M^{I}$ (M = Cu, Ag, Au) Heteronuclear Alkynyl Complexes Prepared by Reaction of $[Pt(C{\equiv}CR)_4]^{2-}$ with $[M_2(dppm)_2]^{2+}$ (dppm = Bis(diphenylphosphino)methane)

Gang-Qiang Yin,[†] Qiao-Hua Wei,[†] Li-Yi Zhang,[†] and Zhong-Ning Chen*[,†,‡]

State Key Laboratory of Structural Chemistry, Fujian Institute of Research on the Structure of Matter and Graduate School of CAS, the Chinese Academy of Sciences, Fuzhou, Fujian 350002, China, and State Key Laboratory of Organometallic Chemistry, Shanghai Institute of Organic Chemistry, The Chinese Academy of Sciences, Shanghai 200032, China

Received July 25, 2005

A series of PtM, PtM_2, and Pt_2M_3 (M = Cu, Ag, Au) heteronuclear alkynyl complexes, synthesized by reaction of the tetraalkynylplatinate(II) complexes $[Pt(C{\equiv}CR)_4]^{2-}$ with $[M_2(\mu\text{-dppm})_2]^{2+}$ (dppm = bis(diphenylphosphino)methane), were characterized by elemental analyses, ESI-MS, ^1H and ^{31}P NMR spectroscopy, and X-ray crystallography for **5**−**13**. The Pt^{II} and M^{I} centers are linked doubly and singly by dppm in the PtM and PtM_2 complexes, respectively. The Pt_2Ag_3 complex **13** is composed of two PtAg units associated with another Ag center by acetylide η^2 (π) coordination. Strong Pt−M bonding interactions are operative, in view of their rather short distances (2.7−3.0 Å). Compounds **1**−**13** emit strongly in the solid state at 298 and 77 K with lifetimes in the microsecond range, indicating spin-forbidden triplet excited states. They also exhibit moderate photoluminescence in degassed dichloromethane at 298 K. The emission energy in the solid state decreases with an increase in the electron-donating ability of the R substituents, implying that the emissive origin is probably substantial ligand-to-cluster [RC≡C→PtM] LMMCT transitions, in view of the Pt−M interactions.

Introduction

Considerable attention has been paid to the chemistry of $Pt^{II}-M^{I}$ (M = Cu, Ag, Au) heterometallic alkynyl complexes in recent years, primarily arising from their intriguing spectroscopic behavior, rich photophysical properties, and diversified structural topology.[1−9] One of the most intriguing features in these complexes is the tendency to form d^8-d^{10} metal−metal contacts that frequently induce intriguing spectroscopic and optoelectronic properties. It has been demonstrated that participation of the phosphine ligands usually favors formation of ligand-bridged or -unsupported $Pt^{II}-M^{I}$ clusters through d^8-d^{10} metal−metal interactions.[1−11]

The tetraalkynylplatinate(II) complexes $[Pt(C{\equiv}CR)_4]^{2-}$ are favorable precursors for construction of the heterometallic alkynyl cluster complexes in terms of their potentially bridging character in the alkynyl ligands through σ or/and π coordination.[12] A series of Pt−Cu,[13] Pt−Ag,[12a,14,15] Pt−Tl,[16] Pt−Cd,[17] and Pt−Rh/Ir[18] heteropolynuclear cluster complexes with $[Pt(C{\equiv}CR)_4]^{2-}$ as building blocks have been isolated, which

* To whom correspondence should be addressed at the Fujian Institute of Research on the Structure of Matter. E-mail: czn@ms.fjirsm.ac.cn.

† Fujian Institute of Research on the Structure of Matter.

‡ Shanghai Institute of Organic Chemistry.

(1) Ara, I.; Berenguer, J. R.; Eguizábal, E.; Forniés, J.; Gómez, J.; Lalinde, E. *J. Organomet. Chem*. **2003**, *670*, 221.

(2) (a) Lang, H.; del Villar, A. *J. Organomet. Chem*. **2003**, *670*, 45. (b) Lang, H.; del Villar, A.; Walfort, B.; Rheinwald, G. *J. Organomet. Chem*. **2004**, *689*, 1464.

(3) (a) Yam, V. W.-W. *J. Organomet. Chem*. **2004**, *689*, 1393. (b) Yam, V. W.-W.; Yu, K.-L.; Wong, K. M.-C.; Cheung, K.-K. *Organometallics* **2001**, *20*, 721. (c) Yam, V. W.-W.; Hui, C.-K.; Wong, K. M.-C.; Zhu, N.; Cheung, K.-K. *Organometallics* **2002**, *21*, 4326.

(4) Adams, C. J.; Raithby, P. R. *J. Organomet. Chem*. **1999**, *578*, 178.

(5) (a) Yamazaki, S.; Deeming, A. J.; Speel, D. M.; Hibbs, D. E.; Hursthouse, M. B.; Malik, K. M. A. *Chem. Commun*. **1997**, 177. (b) Yamazaki, S.; Deeming, A. J. *J. Chem. Soc., Dalton Trans*. **1993**, 3051.

(6) Wong, W.-Y.; Lu, G.-L.; Choi, K.-H. *J. Organomet. Chem*. **2002**, *659*, 107.

(7) (a) Manojlovic-Muir, L.; Henderson, A. N.; Treurnicht, I.; Puddephatt, R. J. *Organometallics* **1989**, *8*, 2055. (b) Smith, D. E.; Welch, A. J.; Treurnicht, I.; Puddephatt, R. J. *Inorg. Chem*. **1986**, *25*, 4616.

(8) Li, Q.-S.; Xu, F.-B.; Cui, D.-J.; Yu, K.; Zeng, X.-S.; Leng, X.-B.; Song, H.-B.; Zhang, Z.-Z. *Dalton Trans*. **2003**, 1551.

(9) Whiteford, J. A.; Stang, P. J.; Huang, S. D. *Inorg. Chem*. **1998**, *37*, 5595.

(10) (a) Wei, Q.-H.; Yin, G.-Q.; Ma, Z.; Shi, L.-X.; Chen, Z.-N. *Chem. Commun*. **2003**, 2188. (b) Wu, M.-M.; Chen, Z.-N. *Chin. J. Struct. Chem*. **2004**, *23*, 1103.

(11) (a) Chen, Y.-D.; Zhang, L.-Y.; Shi, L.-X.; Chen, Z.-N. *Inorg. Chem*. **2004**, *43*, 7493. (b) Chen, Y.-D.; Qin, Y.-H.; Zhang, L.-Y.; Shi, L.-X.; Chen, Z.-N. *Inorg. Chem*. **2004**, *43*, 1197.

(12) (a) Espinet, P.; Forniés, J.; Martinez, F.; Tomás, M.; Lalinde, E.; Moreno, M. T.; Ruiz, A.; Welch, A. J. *J. Chem. Soc., Dalton Trans*. **1990**, 791. (b) Benito, J.; Berenguer, J. R.; Forniés, J.; Gil, B.; Gómez, J.; Lalinde, E. *Dalton Trans*. **2003**, 4331. (c) Falvello, L. R.; Forniés, J.; Gómez, J.; Lalinde, E.; Martín, A.; Moreno, M. T.; Sacristán, J. *Chem. Eur. J*. **1999**, *5*, 474.

(13) (a) Charmant, J. P. H.; Forniés, J.; Gómez, J.; Lalinde, E.; Merino, R. I.; Moreno, M. T.; Orpen, A. G. *Organometallics* **1999**, *18*, 3353. (b) Forniés, J.; Lalinde, E.; Martin, A.; Moreno, M. T. *J. Organomet. Chem*. **1995**, *490*, 179. (c) Yam, V. W.-W.; Yu, K.-L.; Cheung, K.-K. *J. Chem. Soc., Dalton Trans*. **1999**, 2913.

(14) (a) Ara, I.; Forniés, J.; Gómez, J.; Lalinde, E.; Moreno, M. T. *Organometallics* **2000**, *19*, 3137. (b) Ara, I.; Forniés, J.; Gómez, J.; Lalinde, E.; Merino, R. I.; Moreno, M. T. *Inorg. Chem. Commun*. **1999**, *2*, 62.

(15) Yam, V. W.-W.; Hui, C.-K.; Yu, S.-Y.; Zhu, N. *Inorg. Chem*. **2004**, *43*, 812.

(16) Berengue, J. R.; Forniés, J.; Gómez, J.; Lalinde, E.; Moreno, M. T. *Organometallics* **2001**, *20*, 4847.

(17) (a) Charmant, J. P. H.; Falvello, L. R.; Forniés, J.; Gómez, J.; Lalinde, E.; Moreno, M. T.; Orpen, A. G.; Rueda, A. *Chem. Commun*. **1999**, 2045. (b) Forniés, J.; Gómez, J.; Lalinde, E.; Moreno, M. T. *Inorg. Chem*. **2001**, *40*, 5415.

(18) (a) Berenguer, J. R.; Eguizábal, E.; Falvello, L. R.; Forniés, J.; Gómez, J.; Lalinde, E.; Martín, A. *Organometallics* **2000**, *19*, 490. (b) Ara, I.; Berenguer, J. R.; Eguizábal, E.; Forniés, J.; Lalinde, E. *Organometallics* **2001**, *20*, 2686. (c) Ara, I.; Berenguer, J. R.; Fornies, J.; Lalinde, E.; *Organometallics* **1997**, *16*, 3921.

10.1021/om050620e CCC: $33.50
Publication on Web 01/05/2006

exhibit intriguing photophysical properties associated with the metal−metal and η^2−M bonding interactions.

We have been interested in design of $Pt^{II}-M^{I}$ heterometallic cluster complexes that display d^8-d^{10} metal−metal interactions and long-lived luminescence by incorporation of the Pt^{II} thiolate or alkynyl components with the M^{I} diphosphine complexes.[10,11] Reaction of Pt(diimine)(dithiolate) with $[M_2(\mu\text{-dppm})_2]^{2+}$ gave rise to the formation of a series of $Pt^{II}-M^{I}$ heteronuclear cluster thiolate complexes with diverse structures and intriguing photoluminescence.[11] To promote this research, we have attempted to investigate the reactions of $[Pt(C{\equiv}CR)_4]^{2-}$ with $[M_2(\mu\text{-}Ph_2PXPPh_2)_2]^{2+}$ (X = NH, CH_2).[10a] The neutral heterohexanuclear compounds $Pt_2Ag_4(PPh_2NPPh_2)_4(C{\equiv}CC_6H_4R\text{-}p)_4$ (R = H, CH_3) and $[PtAg_2(dppm)_2(C{\equiv}CC_6H_5)_2(CH_3CN)_2](SbF_6)_2$ (**2**; dppm = bis(diphenylphosphino)methane) have been described in a preliminary communication.[10a] We report herein a systematic study on the preparation, structural and spectroscopic characterization, and photoluminescence of a series of $Pt^{II}-M^{I}$ (M = Cu, Ag, Au) heteronuclear complexes derived from the combination between $[Pt(C{\equiv}CR)_4]^{2-}$ and $[M_2(\mu\text{-dppm})_2]^{2+}$.

Experimental Section

Materials and Reagents. All synthetic operations were performed under a dry argon atmosphere by using Schlenk techniques and vacuum-line systems. Solvents were dried by standard methods and distilled prior to use. The reagents bis(diphenylphosphino)methane (dppm), phenylacetylene ($HC{\equiv}CC_6H_5$), 4-ethynyltoluene ($HC{\equiv}CC_6H_4CH_3$-4), 1-ethynyl-4-methoxybenzene ($HC{\equiv}CC_6H_4OCH_3$-4), 4-(*tert*-butyl)phenylacetylene ($HC{\equiv}CC_6H_4Bu^t$-4), (trimethylsilyl)acetylene ($HC{\equiv}CSiMe_3$), and *tert*-butylacetylene ($HC{\equiv}CBu^t$) were available commercially (Acros and Alfa Aesar). The tetraalkynylplatinate(II) compounds $[NBu_4]_2[Pt(C{\equiv}CR)_4]$ (R = C_6H_5, $C_6H_4CH_3$-4, $C_6H_4OCH_3$-4, $C_6H_4Bu^t$-4, ^{t}Bu, $SiMe_3$) were prepared by the literature methods.[12] The precursor compounds $[Cu_2(dppm)_2(MeCN)_2](ClO_4)_2$, $[Ag_2(dppm)_2(MeCN)_2](SbF_6)_2$, and $[Au_2(dppm)_2](SbF_6)_2$ were accessible by similar synthetic procedures in the literature.[19−22]

$[PtAg(dppm)_2(C{\equiv}CC_6H_5)_2](SbF_6)$ (1) and $[PtAg_2(dppm)_2(C{\equiv}CC_6H_5)_2(CH_3CN)_2](SbF_6)_2$ (2). $[Ag_2(dppm)_2(MeCN)_2](SbF_6)_2$ (153.4 mg, 0.10 mmol) was added to a dichloromethane (20 mL) solution of $[NBu_4]_2[Pt(C{\equiv}CC_6H_5)_4]$ (108.4 mg, 0.10 mmol) with stirring at room temperature for 1 day. The clear yellow-green solution was concentrated in vacuo and chromatographed on a silica gel column. The yellow-green band was collected using dichloromethane as an eluent. Compound **1** (yield 64%) was isolated as yellow-green crystals by layering petroleum ether onto the dichloromethane solution. Diffusion of diethyl ether onto the dichloromethane−acetonitrile (5/1 v/v) solutions over a few days, however, gave compound **2** (yield 40%) as yellow crystals and a small amount of yellow-green crystals of **1** (yield 10%).

1. Anal. Calcd for $C_{66}H_{54}AgF_6P_4PtSb{\cdot}2CH_2Cl_2$: C, 48.63; H, 3.48. Found: C, 48.47; H, 3.33. ES-MS (*m*/*z* (%)): 1273 (100) $[M - SbF_6]^+$, 889 (32) $[PtAg(dppm)(C{\equiv}CC_6H_5)_2]^+$. IR (KBr, cm^{-1}): ν 2116 (w, C≡C), 2104 (w, C≡C), 658 (s, SbF_6). ^{1}H NMR (CD_3Cl, ppm): δ 7.76−6.35 (m, 50H, C_6H_5), 5.20 (s, 4H, CH_2Cl_2), 4.14 (s, 4H, PCH_2P). ^{31}P NMR (202.3 MHz, CH_2Cl_2, ppm): 11.8 (s, J_{Pt-P} = 1254 Hz, $PtPCH_2PAg$), 2.2 (d of d, J_{Ag-P} = 528 Hz, $^2J_{P-P}$ = 35 Hz, $PtPCH_2PAg$).

2. Anal. Calcd for $C_{70}H_{60}Ag_2F_{12}N_2P_4PtSb_2$: C, 43.44; H, 3.12; N, 1.45. Found: C, 43.58; H, 3.09; N, 1.34. ES-MS (*m*/*z* (%)): 1273 (100) $[PtAg(dppm)_2(C{\equiv}CC_6H_5)_2]^+$, 889 (30) $[PtAg(dppm)(C{\equiv}CC_6H_5)_2]^+$. IR (KBr, cm^{-1}): ν 2102 (w, C≡C), 2058 (w, C≡C), 658 (s, SbF_6). ^{1}H NMR ($CDCl_3$, ppm): δ 7.74−6.35 (m, 50H, C_6H_5), 4.12 (s, 4H, PCH_2P), 1.63 (s, 6H, CH_3CN). ^{31}P NMR (202.3 MHz, CD_3CN, ppm): 11.8 (s, J_{Pt-P} = 1250 Hz, $PtPCH_2PAg$), 2.3 (d, J_{Ag-P} = 528 Hz, $PtPCH_2PAg$).

$[PtAg(dppm)_2(C{\equiv}CC_6H_4CH_3\text{-}4)_2](SbF_6)$ (3). The synthetic procedure is the same as that of **1**, except using $[NBu_4]_2[Pt(C{\equiv}CC_6H_4CH_3\text{-}4)_4]$ instead of $[NBu_4]_2[Pt(C{\equiv}CC_6H_5)_4]$. Yield: 55%. Anal. Calcd for $C_{68}H_{58}AgF_6P_4PtSb{\cdot}CH_2Cl_2$: C, 51.07; H, 3.73. Found: C, 51.47; H, 3.50. ES-MS (*m*/*z* (%)): 1301 (100) $[M - SbF_6]^+$, 917 (10) $[PtAg(dppm)(C{\equiv}CC_6H_4CH_3\text{-}4)_2]^+$. IR (KBr, cm^{-1}): ν 2116 (w, C≡C), 2089 (w, C≡C), 658 (s, SbF_6). ^{1}H NMR ($CDCl_3$, ppm): δ 7.84−6.25 (m, 48H, C_6H_5 and C_6H_4), 5.24 (s, 2H, CH_2Cl_2), 4.12 (s, 4H, PCH_2P), 2.20 (s, 6H, CH_3). ^{31}P NMR (202.3 MHz, $CDCl_3$, ppm): 12.0 (s, J_{Pt-P} = 1265 Hz, $PtPCH_2PAg$), 2.7 (d of d, J_{Ag-P} = 524 Hz, $^2J_{P-P}$ = 34 Hz, $PtPCH_2PAg$).

$[PtAg(dppm)_2(C{\equiv}CC_6H_4OCH_3\text{-}4)_2](SbF_6)$ (4). The synthetic procedure is the same as that of **1**, except using $[NBu_4]_2[Pt(C{\equiv}CC_6H_4OCH_3\text{-}4)_4]$ instead of $[NBu_4]_2[Pt(C{\equiv}CC_6H_5)_4]$. Yield: 66%. Anal. Calcd for $C_{68}H_{58}AgF_6O_2P_4PtSb{\cdot}CH_2Cl_2$: C, 50.08; H, 3.65. Found: C, 50.64; H, 3.91. ES-MS (*m*/*z* (%)): 1333 (100) $[M - SbF_6]^+$, 949 (25) $[PtAg(dppm)(C{\equiv}CC_6H_4OCH_3\text{-}4)_2]^+$. IR (KBr, cm^{-1}): ν 2119 (w, C≡C), 2090 (w, C≡C), 658 (s, SbF_6).^{1}H NMR ($CDCl_3$, ppm): δ 7.74−6.27 (m, 48H, C_6H_5 and C_6H_4), 4.11 (s, 4H, PCH_2P), 5.22 (s, 2H, CH_2Cl_2), 3.71 (s, 6H, OCH_3). ^{31}P NMR (202.3 MHz, $CDCl_3$, ppm): 12.0 (t, J_{Pt-P} = 1274 Hz, $^2J_{P-P}$ = 35 Hz, $PtPCH_2PAg$), 2.3 (d of d, J_{Ag-P} = 525 Hz, $^2J_{P-P}$ = 30 Hz, $PtPCH_2PAg$).

$[PtAg(dppm)_2(C{\equiv}CBu^t)_2](SbF_6)$ (5). The synthetic procedure is the same as that of **1**, except using $[NBu_4]_2[Pt(C{\equiv}CBu^t)_4]{\cdot}2H_2O$ instead of $[NBu_4]_2[Pt(C{\equiv}CC_6H_5)_4]$. Yield: 46%. Anal. Calcd for $C_{62}H_{62}AgF_6P_4PtSb$: C, 50.67; H, 4.25. Found: C, 50.87; H, 3.96. ES-MS (*m*/*z* (%)): 1233 (100) $[M - SbF_6]^+$, 849 (23) $[PtAg(dppm)(C{\equiv}CBu^t)_2]^+$. IR (KBr, cm^{-1}): ν 2120 (w, C≡C), 2090 (w, C≡C), 658 (s, SbF_6). ^{1}H NMR ($CDCl_3$, ppm): δ 7.94−7.02 (m, 40H, C_6H_5), 4.02 (s, 4H, PCH_2P), 0.52 (s, 18H, C_4H_9). ^{31}P NMR (202.3 MHz, $CDCl_3$, ppm): 10.3 (s, J_{Pt-P} = 1287 Hz, $PtPCH_2PAg$), 1.6 (d of d, J_{Ag-P} = 516 Hz, $^2J_{P-P}$ = 31 Hz, $PtPCH_2PAg$).

$[PtCu(dppm)_2(C{\equiv}CC_6H_5)_2](ClO_4)$ (6). $[Cu_2(dppm)_2(MeCN)_2](ClO_4)_2$ (235.4 mg, 0.20 mmol) was added to a dichloromethane (20 mL) solution of $[NBu_4]_2[Pt(C{\equiv}CC_6H_5)_4]$ (108.8 mg, 0.10 mmol) with stirring for 1 day. The clear orange solution was concentrated in vacuo and chromatographed on a silica gel column. The product was eluted using dichloromethane/acetone (100/1 v/v) and recrystallized in dichloromethane−petroleum ether to give yellow-green crystals. Yield: 51% (75 mg). Anal. Calcd for $C_{66}H_{54}ClCuP_4PtO_4{\cdot}{}^3/_2CH_2Cl_2$: C, 55.66; H, 3.94. Found: C, 55.93; H, 3.68. ES-MS (*m*/*z* (%)): 1229 (100) $[M - ClO_4]^+$, 845 (5) $[PtCu(dppm)(C{\equiv}CC_6H_5)_2]^+$. IR (KBr, cm^{-1}): ν 2116 (w, C≡C), 2079 (w, C≡C), 1100 (s, ClO_4). ^{1}H NMR ($CDCl_3$, ppm): δ 7.76−6.29 (m, 50H, C_6H_5), 5.29 (s, 3H, CH_2Cl_2), 4.07 (s, 4H, PCH_2P). ^{31}P NMR (202.3 MHz, $CDCl_3$, ppm): 13.6 (s, J_{Pt-P} = 1221 Hz, $PtPCH_2PCu$), −5.8 (s, $PtPCH_2PCu$).

$[PtCu_2(dppm)_2(C{\equiv}CC_6H_5)_2(CH_3CN)_2](ClO_4)_2$ (7). To an acetonitrile (20 mL) solution of $[NBu_4]_2[Pt(C{\equiv}CC_6H_5)_4]$ (108.8 mg, 0.10 mmol) was added $[Cu_2(dppm)_2(MeCN)_2](ClO_4)_2$ (235.4 mg, 0.20 mmol) with stirring at room temperature for 1 day. The yellow solution was filtered to remove a small amount of precipitate. Layering diethyl ether onto the concentrated acetonitrile solution afforded yellow crystals in a few days. Yield: 20% (32 mg). Anal. Calcd for $C_{70}H_{60}Cl_2Cu_2N_2O_8P_4Pt$: C, 53.41; H, 3.84; N, 1.78. Found: C, 53.62; H, 3.70; N, 1.63. ES-MS (*m*/*z* (%)): 1229 (100) $[PtCu(dppm)_2(C{\equiv}CC_6H_5)_2]^+$, 886 (35) $[PtCu(dppm)(C{\equiv}CC_6H_5)_2(CH_3CN)]^+$, 845 (20) $[PtCu(dppm)(C{\equiv}CC_6H_5)_2]^+$. IR (KBr, cm^{-1}):

(19) Diez, J.; Gamasa, M. P.; Gimeno, J.; Tiripicchio, A.; Camellini, M. T. *J. Chem. Soc., Dalton Trans.* **1987**, 1275.
(20) Ho, D. M.; Bau, R. *Inorg. Chem.* **1983**, *22*, 4073.
(21) Lin, I. J. B.; Hwang, J. M.; Feng, D.-F.; Cheng, M. C.; Wang, Y. *Inorg. Chem.* **1994**, *33*, 3467.
(22) Che, C.-M.; Kwong, H.-L.; Poon, C.-K.; Yam, V. W.-W. *J. Chem. Soc., Dalton Trans.* **1990**, 3215.

ν 2116 (w, C≡C), 2079 (w, C≡C), 1099 (s, ClO_4). ^1H NMR ($CDCl_3$, ppm): δ 7.76−6.29 (m, 50H, C_6H_5), 4.08 (s, 4H, PCH_2P), 1.67 (s, 6H, CH_3CN). ^{31}P NMR (202.3 MHz, $CDCl_3$, ppm): 13.3 (t, J_{Pt-P} = 1222 Hz; $^2J_{P-P}$ = 34 Hz, Pt*P*CH_2PCu), −5.7 (t, J_{P-P} = 30 Hz, $PtPCH_2PCu$).

[PtCu(dppm)$_2$(C≡CC$_6$H$_4$CH$_3$-4)$_2$](ClO$_4$) (8). This compound was prepared by the same procedure as that of **6**, except using $[NBu_4]_2[Pt(C{\equiv}CC_6H_4CH_3\text{-}4)_4]$ instead of $[NBu_4]_2[Pt(C{\equiv}CC_6H_5)_4]$. The product was eluted using dichloromethane/acetone (50/1 v/v). Yield: 68%. Anal. Calcd for $C_{68}H_{58}ClCuO_4P_4Pt{\cdot}2CH_2Cl_2$: C, 55.06; H, 4.09. Found: C, 55.56; H, 4.20. ES-MS (*m*/*z* (%)): 1257 (100) $[M - ClO_4]^+$, 873 (20) $[PtCu(dppm)(C{\equiv}CC_6H_4CH_3\text{-}4)_2]^+$. IR (KBr, cm^{-1}): ν 2117 (w, C≡C), 2077 (w, C≡C), 1100 (s, ClO_4). ^1H NMR (CD_3Cl, ppm): δ 7.75−6.19 (m, 48H, C_6H_5 and C_6H_4), 5.28 (s, 4H, CH_2Cl_2), 4.05 (s, 4H, PCH_2P), 2.19 (s, 6H, CH_3). ^{31}P NMR (202.3 MHz, $CDCl_3$, ppm): 12.6 (t, J_{Pt-P} = 1226 Hz, $^2J_{P-P}$ = 34 Hz, Pt*P*CH_2PCu), −6.6 (t, J_{P-P} = 34 Hz, $PtPCH_2PCu$).

[PtCu(dppm)$_2$(C≡CC$_6$H$_4$OCH$_3$-4)$_2$](ClO$_4$) (9). This compound was prepared by the same procedure as that of **6**, except utilizing $[NBu_4]_2[Pt(C{\equiv}CC_6H_4OCH_3\text{-}4)_4]$ instead of $[NBu_4]_2[Pt(C{\equiv}CC_6H_5)_4]$. The product was eluted using dichloromethane/acetone (50/1 v/v). Yield: 65%. Anal. Calcd for $C_{68}H_{58}ClCuO_6P_4Pt$: C, 58.79; H, 4.21. Found: C, 58.86; H, 3.91. ES-MS (*m*/*z* (%)): 1289 (100) $[M - ClO_4]^+$, 905 (10) $[PtCu(dppm)(C{\equiv}CC_6H_4OCH_3\text{-}4)_2]^+$. IR (KBr, cm^{-1}): ν 2119 (w, C≡C), 2077 (w, C≡C), 1099 (s, ClO_4). ^1H NMR ($CDCl_3$, ppm): δ 7.74−6.20 (m, 48H, C_6H_5 and C_6H_4), 4.04 (s, 4H, PCH_2P), 3.69 (s, 6H, OCH_3). ^{31}P NMR (202.3 MHz, $CDCl_3$, ppm): 13.1 (t, J_{Pt-P} = 1234 Hz, $^2J_{P-P}$ = 35 Hz, Pt*P*CH_2PCu), −6.6 (t, J_{P-P} = 31 Hz, $PtPCH_2PCu$).

[PtCu(dppm)$_2$(C≡CBu^t)$_2$](ClO$_4$)$_{2/3}$(SbF$_6$)$_{1/3}$ (10). $[Cu_2(dppm)_2(MeCN)_2](ClO_4)_2$ (117.7 mg, 0.10 mmol) was added to a dichloromethane (20 mL) solution of $[NBu_4]_2[Pt(C{\equiv}CBu^t)_4]{\cdot}2H_2O$ (104.1 mg, 0.10 mmol). The solution was stirred at room temperature for 1 day to afford a clear yellow solution, which was concentrated in vacuo and chromatographed on a silica gel column. Elution with dichloromethane/acetone (10/1 v/v) afforded a yellow product. Metathesis of perchlorate with a methanol solution of sodium hexafluoroantimonate afforded compound **10** as pale yellow crystals by diffusion of diethyl ether. Yield: 75 mg (62%). Anal. Calcd for $C_{62}H_{62}CuP_4Pt(ClO_4)_{2/3}(SbF_6)_{1/3}{\cdot}{}^7/_6H_2O$: C, 54.93; H, 4.78. Found: C, 54.67; H, 4.90. ES-MS (*m*/*z* (%)): 1189 (40) $[M - (ClO_4)_{2/3} - (SbF_6)_{1/3}]^+$, 805 (43) $[PtCu(dppm)(C{\equiv}CBu^t)_2]^+$. IR (KBr, cm^{-1}): ν 2006 (w, C≡C), 1099 (s, ClO_4), 659 (s, SbF_6). ^1H NMR (CD_3COCD_3, ppm): δ 7.88−7.23 (m, 40H, C_6H_5), 4.24 (s, 4H, PCH_2P), 0.41 (s, 18H, C_4H_9). ^{31}P NMR (202.3 MHz, $(CD_3)_2CO$, ppm): 12.6 (t, J_{Pt-P} = 1244 Hz, $^2J_{P-P}$ = 31 Hz, Pt*P*CH_2PCu), −5.2 (s, $PtPCH_2PCu$).

[PtAu(dppm)$_2$(C≡CC$_6$H$_5$)$_2$](SbF$_6$) (11). $[Au_2(dppm)_2(MeCN)_2](SbF_6)_2$ (171.6 mg, 0.10 mmol) was added to a dichloromethane (20 mL) solution of $[NBu_4]_2[Pt(C{\equiv}CC_6H_5)_4]$ (108.8 mg, 0.10 mmol) with stirring at room temperature for 1 day to afford a clear yellow-green solution. Layering *n*-hexane onto the concentrated solutions afforded yellow-green crystals in a few days. Yield: 100 mg (63%). Anal. Calcd for $C_{66}H_{54}AuF_6P_4PtSb{\cdot}{}^1/_2CH_2Cl_2$: C, 48.66; H, 3.38. Found: C, 49.04; H, 3.79. ES-MS (*m*/*z* (%)): 1363 (28) $[M - SbF_6]^+$. IR (KBr, cm^{-1}): ν 2104 (w, C≡C), 659 (s, SbF_6). ^1H NMR ($CDCl_3$, ppm): δ 7.84−6.43 (m, 50H, C_6H_5), 5.29 (s, H, CH_2Cl_2), 4.46 (s, 4H, PCH_2P). ^{31}P NMR (202.3 MHz, $CDCl_3$, ppm): 29.8 (q, $^2J_{P-P}$ = 49 Hz, $^2J'_{P-P}$ = 25 Hz, $PtPCH_2PAu$), 8.3 (t, J_{Pt-P} = 1295 Hz, $^2J_{P-P}$ = 25 Hz, Pt*P*CH_2PAu).

[PtCu$_2$(dppm)$_2$(C≡CSiMe$_3$)$_2$(CH$_3$CN)$_2$](SbF$_6$)$_2$ (12). The reaction was carried out by the same procedure as for **7** using $[NBu_4]_2[Pt(C{\equiv}CSiMe_3)_4]{\cdot}2H_2O$ instead of $[NBu_4]_2[Pt(C{\equiv}CC_6H_5)_4]$. The product was eluted using dichloromethane/acetone (24/1 v/v). Metathesis of perchlorate with sodium hexafluoroantimonate afforded yellow crystals by layering diethyl ether onto the dichloromethane−acetonitrile solution. Yield: 26%. Anal. Calcd for $C_{64}H_{68}Cu_2F_{12}N_2P_4PtSb_2Si_2{\cdot}2CH_2Cl_2$: C, 39.46; H, 3.61; N, 1.39. Found: C, 39.75; H, 3.50; N, 1.41. IR (KBr, cm^{-1}): ν 1974 (w, C≡C), 658 (s, SbF_6). ^1H NMR (CD_3CN, ppm): δ 7.89−7.32 (m, 40H, C_6H_5), 3.92 (s, 4H, PCH_2P), 1.95 (s, 6H, CH_3CN), −0.21 (s, 9H, CH_3), −0.32 (s, 9H, CH_3).

[Pt$_2$Ag$_3$(dppm)$_4$(C≡CC$_6$H$_4$Bu^t-4)$_4$](SbF$_6$)$_3$ (13). $[Ag_2(dppm)_2(MeCN)_2](SbF_6)_2$ (153.4 mg, 0.10 mmol) was added to a dichloromethane (20 mL) solution of $[NBu_4]_2[Pt(C{\equiv}CC_6H_4Bu^t)_4]$ (130.8 mg, 0.10 mmol) with stirring at room temperature for 1 day. The orange solution was concentrated and chromatographed on a silica gel column. Elution with dichloromethane−methanol (100/1 v/v) afforded an orange product. Layering *n*-hexane onto the concentrated dichloromethane solution gave orange crystals. Yield: 30%. Anal. Calcd for $C_{148}H_{140}Ag_3F_{18}P_8Pt_2Sb_3{\cdot}2CH_2Cl_2{\cdot}2CH_3OH{\cdot}4H_2O$: C, 46.89; H, 4.14. Found: C, 47.03; H, 3.95. ES-MS (*m*/*z* (%)): 1386 (100) $[PtAg(dppm)_2(C{\equiv}CC_6H_4C_4H_9)_2]^+$. IR (KBr, cm^{-1}): ν 2106 (w, C≡C), 658 (s, SbF_6).^1H NMR ($CDCl_3$, ppm): δ 7.74−6.31 (m, 96H, C_6H_5 and C_6H_4), 4.11 (s, 8H, PCH_2P), 1.35−0.98 (m, 36H, C_4H_9). ^{31}P NMR (202.3 MHz, CD_3CN, ppm): 11.5 (t, J_{Pt-P} = 1262 Hz, $^2J_{P-P}$ = 32 Hz, Pt*P*CH_2PAg), 2.4 (d of d, J_{Ag-P} = 526 Hz, $^2J_{P-P}$ = 30 Hz).

Crystal Structure Determination. Crystals coated with epoxy resin or sealed in capillaries with mother liquors were measured on a Siemens SMART CCD diffractometer by the ω-scan technique at room temperature using graphite-monochromated Mo Kα (λ = 0.710 73 Å) radiation. An absorption correction by SADABS was applied to the intensity data. The structures were solved by direct methods or Patterson procedures, and the heavy atoms were located from an *E* map. The remaining non-hydrogen atoms were determined from the successive difference Fourier syntheses. All non-hydrogen atoms were refined anisotropically, except for those mentioned. The hydrogen atoms were generated geometrically with isotropic thermal parameters. The structures were refined on F^2 by full-matrix least-squares methods using the SHELXTL-97 program package.[23] Crystallographic data were summarized in Table 1 for **5**−**9** and in Table 2 for **10**−**13**. Full crystallographic data are provided in the Supporting Information. In addition, a crystallographic analysis for compound **1** was also carried out, but the results were not entirely satisfactory because of the poor quality of the crystals.

Physical Measurements. Elemental analyses (C, H, N) were carried out on a Perkin-Elmer Model 240C automatic instrument. Electrospray ion mass spectra (ESI-MS) were recorded on a Finnigan LCQ mass spectrometer using dichloromethane−methanol or acetonitrile−methanol as the mobile phase. UV−vis absorption spectra were measured on a Perkin-Elmer Lambda 25 UV−vis spectrometer. Infrared spectra were recorded on a Magna750 FT-IR spectrophotometer with KBr pellets. ^1H and ^{31}P NMR spectra were measured on a Varian UNITY-500 spectrometer with $SiMe_4$ as the internal reference and 85% H_3PO_4 as the external standard, respectively. Emission and excitation spectra were recorded on a Perkin-Elmer LS 55 luminescence spectrometer with a red-sensitive photomultiplier, type R928. Emission lifetimes were determined on an Edinburgh Analytical Instrument (F900 fluorescence spectrometer) using an LED laser at 397 nm excitation, and the resulting emission was detected by a thermoelectrically cooled Hamamatsu R3809 photomultiplier tube. The instrument response function at the excitation wavelength was deconvoluted from the luminescence decay.

Results and Discussion

Synthesis and Characterization. As shown in Scheme 1, reactions of $[Pt(C{\equiv}CR)_4]^{2-}$ (R = C_6H_5, $C_6H_4CH_3$-4, $C_6H_4OCH_3$-4, $C_6H_4Bu^t$-4, Bu^t, $SiMe_3$) with 1 or 2 equiv of $[M_2$-

(23) Sheldrick, G. M. SHELXL-97, Program for the Refinement of Crystal Structures; University of Göttingen, Göttingen, Germany, 1997.

Table 1. Crystallographic Data for Compounds $5\cdot 2CH_2Cl_2$, $6\cdot {}^3/_2CH_2Cl_2$, 7, $8\cdot 2CH_2Cl_2$, and $9\cdot CH_2Cl_2$

	$5\cdot 2CH_2Cl_2$	$6\cdot {}^3/_2CH_2Cl_2$	7	$8\cdot 2CH_2Cl_2$	$9\cdot CH_2Cl_2$
empirical formula	$C_{64}H_{66}AgCl_4F_6P_4SbPt$	$C_{67.5}H_{57}CuCl_4O_4P_4Pt$	$C_{70}H_{60}Cl_2Cu_2O_8N_2P_4Pt$	$C_{70}H_{62}Cl_5CuO_4P_4Pt$	$C_{69}H_{60}Cl_3CuO_6P_4Pt$
fw	1639.56	1456.44	1574.14	1526.96	1474.03
space group	*C*2/*m*	$P2_1/n$	$P2_1/c$	$P2_1/n$	$P2_1/c$
a, Å	42.5886(4)	10.6906(2)	14.3979(2)	10.6760(2)	19.752(4)
b, Å	15.4091(3)	25.2092(5)	14.182(1)	25.4950(5)	15.376(3)
c, Å	21.9684(3)	23.8996(3)	17.5610(3)	24.5754(1)	21.190(5)
β, deg	107.045(1)	100.097(1)	109.723(1)	101.592(1)	97.952(2)
V, Å^3	13783.5(4)	6341.22(19)	3375.46(7)	6552.61(18)	6374(2)
Z	8	4	2	4	4
ρ_{calcd}, g/cm^3	1.580	1.526	1.549	1.548	1.536
μ, mm^{-1}	2.996	2.856	2.921	2.807	2.804
radiation (λ, Å)	0.710 73	0.710 73	0.710 73	0.710 73	0.710 73
temp, K	293(2)	293(2)	293(2)	293(2)	293(2)
R1 (F_o)[a]	0.0630	0.0574	0.0734	0.0746	0.0495
wR2 (F_o^2)[b]	0.1514	0.1333	0.1594	0.1719	0.1290
GOF	1.128	1.109	1.227	1.294	1.097

[a] $R1 = \sum|F_o - F_c|/\sum F_o$. [b] $wR2 = \sum[w(F_o^2 - F_c^2)^2]/\sum[w(F_o^2)]^{1/2}$.

Table 2. Crystallographic Data for Compounds $10\cdot {}^7/_6H_2O$, $11\cdot {}^1/_2CH_2Cl_2$, $12\cdot 2CH_2Cl_2$, and $13\cdot 2CH_2Cl_2\cdot 2CH_3OH\cdot 4H_2O$

	$10\cdot {}^7/_6H_2O$	$11\cdot {}^1/_2CH_2Cl_2$	$12\cdot 2CH_2Cl_2$	$13\cdot 2CH_2Cl_2\cdot 2CH_3OH\cdot 4H_2O$
empirical formula	$C_{62}H_{64.33}Cl_{0.67}CuF_2O_{3.83}P_4PtSb_{0.33}$	$C_{66.5}H_{56}AuClF_6P_4SbPt$	$C_{66}H_{72}Cl_4Cu_2F_{12}N_2Si_2P_4Pt\ Sb_2$	$C_{152}H_{158}Ag_3Cl_4F_{18}O_6P_8Sb_3Pt_2$
fw	1355.53	1642.25	2008.78	3891.38
space group	*R*3*c*	$P\bar{1}$	$P2_1/c$	*C*2/*c*
a, Å	22.7865(2)	11.2890(2)	14.9699(4)	38.3167(1)
b, Å	22.7865(2)	14. 7199(3)	15.0645(4)	20.9887(2)
c, Å	67.5519(1)	20.5532(4)	18.2548(4)	29.0955(2)
α, deg		81.33(1)		
β, deg	120	79.603(1)	104.526(1)	129.498(1)
γ, deg		71.900(1)		
V, Å^3	30375.5(4)	3176.67(11)	3985.12(17)	18055.8(2)
Z	18	2	2	4
ρ_{calcd}, g/cm^3	1.334	1.717	1.674	1.432
μ, mm^{-1}	2.682	5.122	3.254	2.497
radiation (λ, Å)	0.710 73	0.710 73	0.710 73	0.710 73
temp, K	293(2)	293(2)	293(2)	293(2)
R1 (F_o)[a]	0.0596	0.0864	0.0701	0.0790
wR2 (F_o^2)[b]	0.1539	0.1966	0.1701	0.1947
GOF	1.137	1.232	1.167	1.165

[a] $R1 = \sum|F_o - F_c|/\sum F_o$. [b] $wR2 = \sum[w(F_o^2 - F_c^2)^2]/\sum[w(F_o^2)]^{1/2}$.

Scheme 1. Synthetic Routes to the Pt^{II}-M^{I} Heteronuclear Complexes

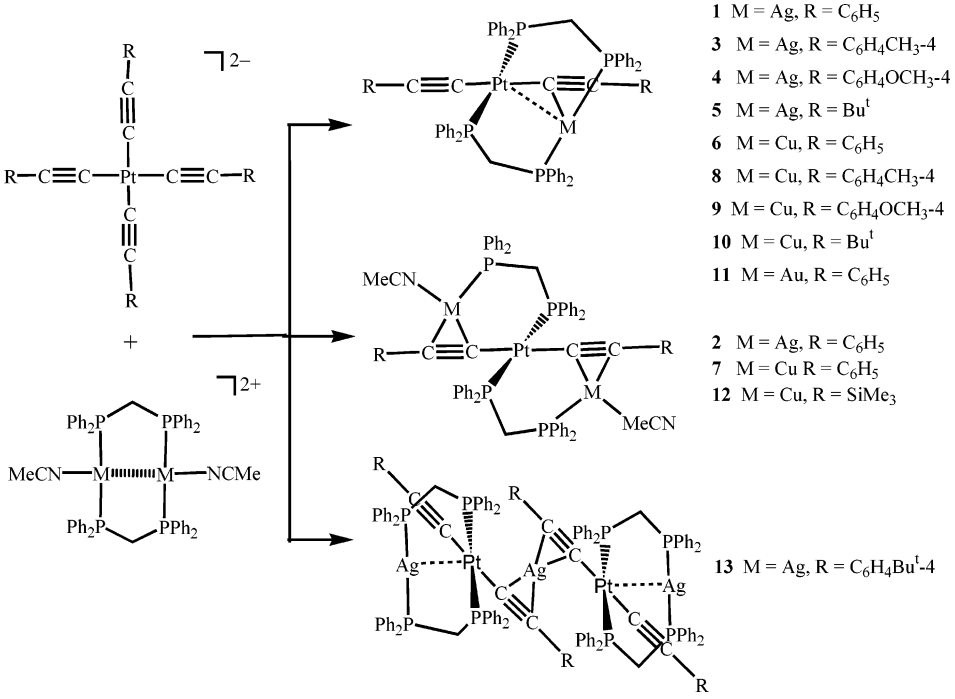

$(dppm)_2(MeCN)_2]^{2+}$ (M = Cu^I, Ag^I, Au^I) afforded three types of $Pt^{II}-M^{I}$ heteronuclear complexes with different structural topologies. It appears that the solvents and solution concentrations play a major role in determining the nuclearity of the PtM, PtM_2, and Pt_2M_3 complexes. Layering *n*-hexane or petroleum ether onto the dichloromethane solutions induced formation of

Table 3. Selected Bond Distances (Å) and Angles (deg) for Complexes 5−9

5		6		7		8		9	
				Pt−M					
Pt1−Ag1	2.9805(11)	Pt−Cu	2.7384(11)	Pt−Cu	3.413 (12)	Pt−Cu	2.7265(14)	Pt−Cu	2.7388(9)
				Pt−C					
Pt1−C11	2.030(16)	Pt−C11	2.025(9)	Pt−C11	2.024(12)	Pt−C11	2.022(10)	P−C11	2.016(6)
Pt1−C21	2.025(17)	Pt−C21	1.993(9)			Pt−C21	2.018(11)	P−C21	1.995(7)
				Pt−P					
Pt1−P2	2.308(3)	Pt−P2	2.316(2)	Pt−P2	2.317(3)	Pt−P2	2.303(3)	Pt−P2	2.3004(16)
		Pt−P4	2.309(2)			Pt−P4	2.314(3)	Pt−P4	2.2945(15)
				M−C					
Ag1−C11	2.523(15)	Cu−C11	2.251(9)	Cu−C11	2.106(11)	Cu−C11	2.269(10)	Cu−C11	2.206(6)
				Cu−C12	2.151(12)				
				M−P					
Ag1−P1	2.393(3)	Cu−P1	2.239(3)	Cu−P1	2.287(3)	Cu−P1	2.237(3)	Cu−P1	2.2332(18)
		Cu−P3	2.251(3)	Cu−N1	1.958(12)	Cu−P3	2.233(3)	Cu−P3	2.2281(18)
				C≡C					
C11−C12	1.20(2)	C11−C12	1.231(12)	C11−C12	1.225(15)	C11−C12	1.216(14)	C11−C12	1.218(9)
C21−C22	1.20(2)	C21−C22	1.216(12)			C21−C22	1.191(15)	C21−C22	1.205(9)
				C−Pt−C					
C11−Pt1−C21	167.1(6)	C11−Pt−C21	172.5(3)	C11−Pt−C11A	180.0(9)	C11−Pt−C21	173.5(4)	C11−Pt−C21	169.4(2)
				C−Pt−P					
C21−Pt1−P2	89.85(7)	C11−Pt−P4	90.6(2)	C11−Pt−P2	90.8(3)	C11−Pt−P2	89.2(3)	C11−Pt−P2	89.59(16)
C11−Pt1−P2	91.13(7)	C21−Pt−P4	93.0(2)	C11A-Pt−P2	89.2(3)	C21−Pt−P2	93.5(3)	C21−Pt−P2	90.87(17)
C21−Pt1−P2A	89.85(7)	C11−Pt−P2	87.5(2)			C11−Pt−P4	87.8(3)	C11−Pt−P4	88.79(16)
C11−Pt1−P2A	91.13(7)	C21−Pt−P2	89.1(2)			C21−Pt−P4	89.5(3)	C21−Pt−P4	90.84(16)
				P−Pt−P					
P2−Pt1−P2A	171.24(13)	P2−Pt−P4	177.85(8)	P2−Pt−P2A	180.0(15)	P2−Pt−P4	176.96(9)	P2−Pt−P4	178.24(5)
				P−M−P					
P1−Ag1−P1A	165.54(14)	P1−Cu−P3	161.62(10)			P1−Cu−P3	161.08(12)	P1−Cu−P3	162.77(7)
				P−M−C					
P1−Ag1−C11	89.40(8)	P1−Cu−C11	99.3(2)	P1−Cu−C11	109.0(3)	P1−Cu−C11	95.5(3)	P1−Cu−C11	97.19(15)
		P3−Cu−C11	96.0(2)	P1−Cu−C12	142.3(3)	P3−Cu−C11	99.0(3)	P3−Cu−C11	97.52(15)

the yellow-green or pale yellow heterobinuclear $Pt^{II}M^{I}$ complexes $[PtM(dppm)_2(C{\equiv}CR)_2]^+$. The yellow heterotrinuclear $Pt^{II}M^{I}_2$ complexes $[PtM_2(dppm)_2(C{\equiv}CR)_2(MeCN)_2]^{2+}$ (M = Ag, Cu; R = C_6H_5; M = Cu, R = $SiMe_3$), however, were crystallized in acetonitrile or dichloromethane−acetonitrile solutions by diffusion of diethyl ether. Layering *n*-hexane onto a highly concentrated dichloromethane solution gave rise to isolation of the orange $Pt^{II}_2M^{I}_3$ heteropentanuclear complex $[Pt_2Ag_3(dppm)_4(C{\equiv}CR)_4]^{3+}$ (R = $C_6H_4Bu^t$-4).

Compounds **1**−**13** were characterized by elemental analyses, ESI-MS, IR and ^{1}H and ^{31}P NMR spectroscopy, and X-ray crystallography for **5**−**13**. The ESI-MS of the $Pt^{II}M^{I}$ heterobinuclear complexes showed the molecular ion fragments $[M - (SbF_6)]^+$ and $[M - (ClO_4)]^+$ as the principal peaks with high abundance. The $Pt^{II}M^{I}_2$ and $Pt^{II}_2M^{I}_3$ complexes, however, only afforded the fragments $[PtM(dppm)_2(C{\equiv}CR)_2]^+$ as the base peaks, whereas the molecular ion fragments $[M - (SbF_6)_2]^{2+}$/$[M - (ClO_4)_2]^{2+}$ and $[M - (SbF_6)_2]^{3+}$ were undetected for the $Pt^{II}M^{I}_2$ and $Pt^{II}_2M^{I}_3$ complexes, respectively. This probably indicates the instability of the $Pt^{II}M^{I}_2$ and $Pt^{II}_2M^{I}_3$ species in solution under the ESI-MS measurement conditions.

In the ^{31}P NMR spectra of Pt^{II}−M^{I} heteronuclear compounds **1**−**13**, typical P satellite peaks arising from the Pt−P coupling occur at 8.3−13.6 ppm with the J_{Pt-P} value in the range of 1220−1300 Hz.[10a,11] In some cases, the Pt−P satellite signals show a moderate splitting that originates from the P−P couplings through *P*−CH_2−*P* or/and *P*−Pt−*P* pathways with $^2J_{P-P}$ = 30−35 Hz. For Pt^{II}−Ag^{I} heteronuclear compounds **1**−**5** and **13**, the P donors bound to the Ag^{I} centers afford doublets or doublet of doublets centered at 1.6−2.7 ppm because of the effects of both Ag−P and P−P couplings with $^1J_{Ag-P}$ = 515−530 Hz and $^2J_{P-P}$ = 30−35 Hz. In the ^{31}P NMR spectra of Pt^{II}−Cu^{I} compounds **6**−**10** and **12**, the P donors bonded to the Cu^{I} centers are observed at ca. −6.0 ppm as a singlet or triplet due to the presence of the P−P coupling. The P signal of the Au−P donors in the $Pt^{II}Au^{I}$ compound **11** is observed at 29.8 ppm as a quintet due to the P−P coupling through both *P*−CH_2−*P* and *P*−Pt−*P* pathways.

Crystal Structures. The crystal structures of compounds **5**−**13** were determined by X-ray crystallography. Selected bonding parameters are listed in Table 3 for **5**−**9** and in Table 4 for **10**−**13**. ORTEP drawings of **5** (PtAg), **6** (PtCu), **7** ($PtCu_2$), **11** (PtAu), and **13** (Pt_2Ag_3) are depicted in Figures 1−5, respectively.

The PtAg and PtCu complexes exhibit similar structures. The heterobinuclear complex cation consists of a PtM assembly bridged doubly by dppm. The two acetylides adopt different bonding modes. One is bonded to both Pt^{II} and M^{I} centers in an asymmetric μ-η^1:η^1 mode with the Pt−C distance being much shorter than the M−C distance, whereas the other is only bound to the Pt center in an η^1 fashion. The arrays of Pt−C≡C (165.0(13)−178.0(3)°) are quasi-linear, while those of M−C≡C (106.7(5)−114.0(12)°) are curved. The Pt−C−M angles are in the range of 76.8(3)−83.2(5)°. The Pt^{II} center is located in an approximately square-planar environment with trans-oriented C_2P_2 donors, and the M^{I} center is surrounded by a T-type arranged CP_2 chromophore. The Pt−M distances are in the range of 2.946(4)−2.9805(11) and 2.7265(14)−2.767(2) Å for M = Ag, Cu, respectively, demonstrating the presence of strong Pt−M bonding interactions.[24] The dihedral angle between the coordination plane of Pt^{II} and that of the M^{I} center is in the range of 82.1−94.2°.

The structure of the PtAu compound $[PtAu(dppm)_2(C{\equiv}CC_6H_5)_2](PF_6)$ with hexafluorophosphate instead of hexafluoroantimonate in **11** (Figure 4) has been described in the literature.[25] The molecular structure of the PtAu complex

(24) Pyykkö, P. *Chem. Rev.* **1997**, *97*, 597−636.

Table 4. Selected Bond Distances (Å) and Angles (deg) for Complexes 10−13

10		11		12		13	
				Pt−M			
Pt−Cu	2.767(2)	Pt−Au	2.9271(8)	Pt−Cu	3.473(11)	Pt1−Ag1	3.0013(15)
				Pt−C			
Pt−C11	2.011(12)	Pt−C11	2.067(18)	Pt−C11	1.999(10)	Pt1−C11	1.992(15)
Pt−C21	1.980(14)	Pt−C21	2.033(14)			Pt1−C31	1.982(16)
				Pt−P			
Pt−P2	2.308(4)	Pt−P2	2.308(4)	Pt−P2	2.306(2)	Pt1−P2	2.333(4)
Pt−P4	2.311(4)	Pt−P4	2.315(4)			Pt1−P4	2.329(4)
				M−C			
Cu−C11	2.153(16)			Cu−C11	2.124(11)	Ag2−C11	2.318(16)
				Cu−C12	2.070(12)	Ag2−C12	2.296(16)
				M−P			
Cu−P1	2.226(4)	Au−P1	2.329(4)	Cu−P1	2.555(3)	Ag1−P1	2.403(4)
Cu−P3	2.234(4)	Au−P3	2.322(4)	Cu−N1	1.956(14)	Ag1−P3	2.399(4)
				C≡C			
C11−C12	1.230(16)	C11−C12	1.19(2)	C11−C12	1.224(15)	C11−C12A	1.26(2)
C21−C22	1.205(18)	C21−C22	1.17(2)			C31−C32	1.21(2)
				C−Pt−C			
C11−Pt−C21	170.4(7)	C11−Pt−C21	177.3(6)	C11−Pt−C11A	180.000(1)	C11−Pt1−C31	171.5(6)
				C−Pt−P			
C11−Pt−P2	91.3(4)	C11−Pt−P2	85.6(4)	C11−Pt−P2	89.9(3)	C11−Pt−P2	92.9(4)
C21−Pt−P2	89.3(5)	C11−Pt−P4	93.2(4)	C11A-Pt−P2	90.2(3)	C11−Pt−P4	94.3(4)
C11−Pt−P4	86.0(4)	C21−Pt−P2	95.4(5)			C31−Pt−P2	86.2(4)
C21−Pt−P4	93.4(5)	C21−Pt−P4	86.1(5)			C31−Pt−P4	86.8(4)
				P−Pt−P			
P2−Pt−P4	177.26(16)	P2−Pt−P4	175.72(14)	P2−Pt−P2A	180.0(0)	P2−Pt−P4	172.53(14)
				P−M−P			
P1−Cu−P3	159.49(19)	P1−Au−P3	173.69(15)			P1−Ag1−P3	161.24(17)
				P−M−C			
C11−Cu−P1	100.1(4)			P1−Cu−C11	107.2(3)	C11−Ag2−C12	148.3(5)
C11−Cu−P3	100.2(4)			P1−Cu−C12	140.5(3)	C11−Ag2−C12A	31.7(5)

resembles those of PtAg and PtCu complexes, but both acetylides are only bound to the Pt^{II} center in an η^1 bonding mode instead of μ-η^1:η^1 and η^1 fashions, respectively. While the Pt^{II} center is in a distorted-square-planar geometry with the C_2P_2 chromophore, the Au^{I} center is surrounded by two P donors in an approximately linear arrangement with P−Au−P = 173.69(15)°.

As shown in Scheme 1, while the Pt^{II} and M^{I} centers are linked doubly by two syn-oriented dppm ligands in the PtM

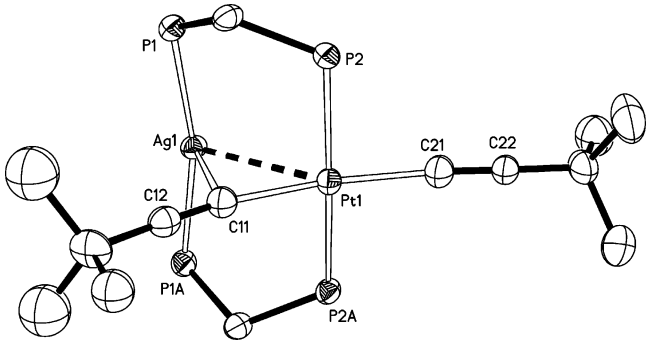

Figure 1. ORTEP drawing of the complex cation of **5**, with the atom-labeling scheme, showing 30% thermal ellipsoids. Phenyl rings on the phosphorus atoms are omitted for clarity.

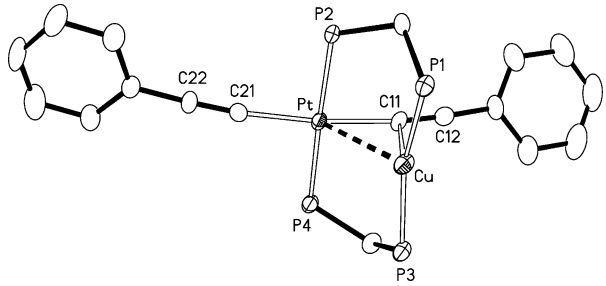

Figure 2. ORTEP drawing of the complex cation of **6**, with the atom-labeling scheme, showing 30% thermal ellipsoids. Phenyl rings on the phosphorus atoms are omitted for clarity.

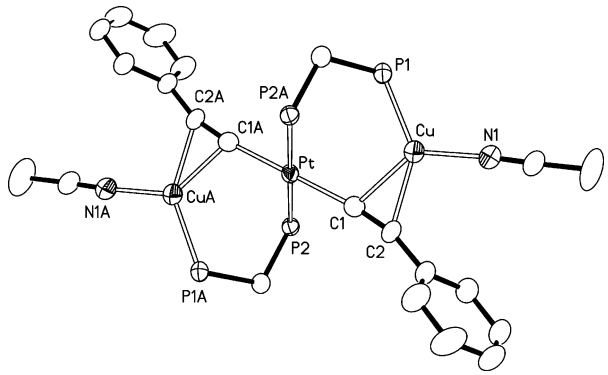

Figure 3. ORTEP drawing of the complex cation of **7**, with the atom-labeling scheme, showing 30% thermal ellipsoids. Phenyl rings on the phosphorus atoms are omitted for clarity.

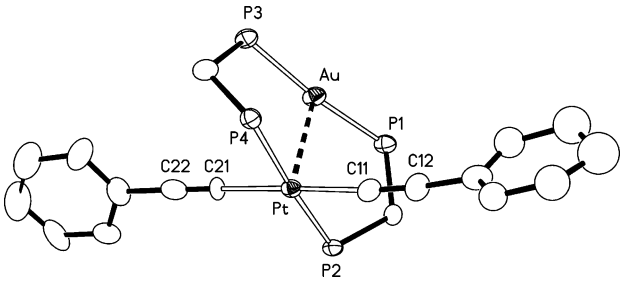

Figure 4. ORTEP drawing of the complex cation of **11**, with the atom-labeling scheme, showing 30% thermal ellipsoids. Phenyl rings on the phosphorus atoms are omitted for clarity.

Table 5. Photophysical Data for Compounds 1−13

compd	λ_{abs}/nm (ϵ/dm^3 mol^{-1} cm^{-1})[a]	medium	λ_{em}/nm (τ_{em}/μs)[b] at 298 K	λ_{em}/nm at 77 K
1	248 (37 922), 270 (35 829), 318 (17 211), 379 (16 850)	solid	481 (3.5)	472, 517 (sh)
		CH_2Cl_2	428 (3.1 ns), 544 (2.9)	463
2	312 (20 800), 376 (18 890)	solid	579 (6.7)	574
		CH_2Cl_2	528 (8.8), 420 (3.6 ns)	549, 493 (sh)
3	256 (39 177), 271 (36 912), 314 (15 935), 383 (16 639)	solid	495 (1.5)	495
		CH_2Cl_2	434 (2.9 ns), 543 (2.8)	473
4	256 (36 293), 271 (32 715), 394 (15 956)	solid	512 (0.8)	514
		CH_2Cl_2	442 (12.3 ns), 540 (0.06)	485
5	241 (41 440), 314 (16 185), 364 (6606)	solid	558 (7.1)	569
		CH_2Cl_2	412 (10.3 ns)	485
6	243 (39 755), 262 (35 411), 354 (12 876), 383 (13 732)	solid	492 (2.0)	481
		CH_2Cl_2	422 (6.7 ns)	475
7	256 (40 256), 280 (34 333), 351 (17 937), 382 (16 532)	solid	500 (1.2), 600	485
		CH_2Cl_2	497 (4.1)	474
8	238 (37 346), 357 (7894), 391 (9458)	solid	496 (3.2)	485
		CH_2Cl_2	434 (6.7 ns)	476
9	264 (41 997), 281 (35 036), 360 (11 538), 403 (16 976)	solid	495 (5.2)	489, 538 (sh)
		CH_2Cl_2	449 (8.1 ns)	495
10	242 (32 698), 276 (14 999), 341 (9752)	solid	509 (6.1)	514
		CH_2Cl_2	415 (11.1 ns)	496
11	246 (38 641), 329 (15 066), 393 (10 348)	solid	484 (0.9)	474, 521 (sh)
		CH_2Cl_2	455 (0.5)	469
12	239 (47 579), 335 (8936)	solid	604 (3.6)	555
		CH_2Cl_2	621 (5.7)	512
13	232 (145 641), 261 (33 944), 380 (39 061)	solid	576 (1.7, 0.3)	567
		CH_2Cl_2	437 (3.2 ns)	543

[a] In CH_2Cl_2 at 298 K. [b] The excitation wavelength in the lifetime measurement is 397 nm.

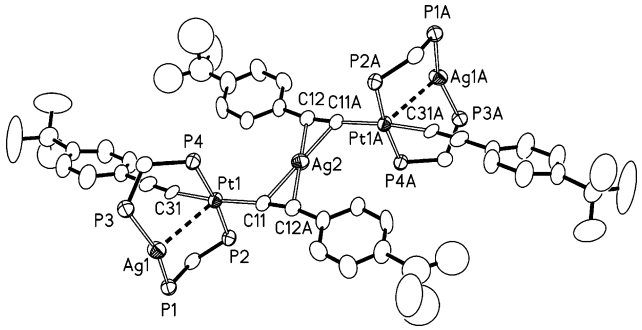

Figure 5. ORTEP drawing of the complex cation of **13**, with the atom-labeling scheme, showing 30% thermal ellipsoids. Phenyl rings on the phosphorus atoms are omitted for clarity.

heterobinuclear complexes, the Pt^{II} and Cu^{I} centers are bridged singly by two anti-arranged dppm ligands to give the quasi-linear heterotrinuclear array in the $PtCu_2$ complex **7** (Figure 3). The acetylide exhibits an μ-η^1:η^2 bonding mode, bound to the Pt^{II} and Cu^{I} centers through σ (η^1) and π (η^2) coordination, respectively. The Pt^{II} center affords a square-planar geometry with trans-oriented C_2P_2 donors, whereas the Cu^{I} center is in a distorted-triangle-planar surrounding formed by the π-bonding acetylide, P donor, and acetonitrile. The Pt···Cu (3.413(12) Å) distance, however, is much longer than that observed in the PtM binuclear complexes. The Cu···Cu separation is more than 6.8 Å.

The Pt_2Ag_3 heteropentanuclear complex **13** (Figure 5) can be viewed as incorporating two $PtAg_2(dppm)_2(C{\equiv}CPh)_2$ components with one Ag^{I} center through acetylide π-coordination. The Pt^{II} center exhibits an approximately square-planar geometry with trans-oriented C_2P_2 donors. The Ag1 and Ag2 centers are located in distorted linear environments built by two P donors and two π-bonded acetylides, respectively. The acetylide C11≡C12A exhibits a μ-η^1:η^2 bonding mode, bound to the Pt^{II} and Ag^{I} centers through σ (η^1) and π (η^2) coordination, respectively. The acetylide C31 donor, however, is η^1-bonded to the Pt^{II} center. While the Pt1−Ag1 (3.0013(15) Å) distance is indicative of the presence of a strong Pt−Ag contact, the Pt1−Ag2 (3.591-(1) Å) distance is much longer. The Pt1···Pt1a and Ag1···Ag2 separations are 7.181(1) and 6.480(1) Å, respectively.

Photophysical Properties. The absorption and emission data of complexes **1**−**13** are summarized in Table 5. The electronic absorption spectra in dichloromethane are characterized by intense bands at ca. 230−280 nm, absorption shoulders in the region of 310−350 nm, and low-energy bands at ca. 365−405 nm. The high-energy bands at ca. 230−280 nm are ascribed to dppm intraligand (IL) transitiona, since the free dppm also absorbs strongly in this region. The absorption shoulders at ca. 310−350 nm are likely to be involved in metal-perturbed π−π* (C≡CR) transitions, since the related monomeric complex [Pt-(dppm-P)$_2$(C≡CPh)$_2$] shows an absorption band at ca. 345 nm, assigned to an admixture of the metal-to-ligand charge transfer [d(Pt) → π*(C≡CPh)] and intraligand π → π* transitions.[25−27] The low-energy bands at ca. 365−405 nm in the complexes **1**−**13** are tentatively ascribed to [d(PtM) → π*(C≡CR)] MLCT transitions, as suggested for the $[PtAu(dppm)_2(C{\equiv}CPh)_2]^+$ complex.[25] The absorption energy of the low-energy bands for **1**, **3**, and **4** with R = aryl is obviously red shifted compared with that for the PtAg heterobinuclear complex **5** with R = Bu^t (Figure 6), due to the better π-electron-accepting ability for the former than the latter. Likewise, the absorption energy of the low-energy band for **6**, **8**, and **9** with R = aryl is also lower than that for the PtCu heterobinuclear complex **10** with R = Bu^t. Interestingly, the low-energy absorption band displays a negative solvatochromism,[28] i.e., a higher energy shift in a more polar solvent, as demonstrated by the absorption spectra of complex **9** in various solvents (Figure 7).

As shown in Table 5, compounds **1**−**13** emit strongly in the solid state and in frozen glasses at 77 K with excitations at λ_{ex}

(25) Yip, H.-K.; Lin, H.-M.; Wang, Y.; Che, C.-M. *J. Chem. Soc., Dalton Trans.* **1993**, 2939.

(26) Langrick, C. R.; McEwan, D. M.; Pringle, P. G.; Shaw, B. L. *J. Chem. Soc., Dalton Trans.* **1983**, 2487.

(27) Sacksteder, L.; Baralt, E.; DeGraff, B. A.; Lukehart, C. M.; Demas, J. N. *Inorg. Chem.* **1991**, *30*, 2468.

(28) Cummings, S. D.; Eisenberg, R. *J. Am. Chem. Soc.* **1996**, *118*, 1949.

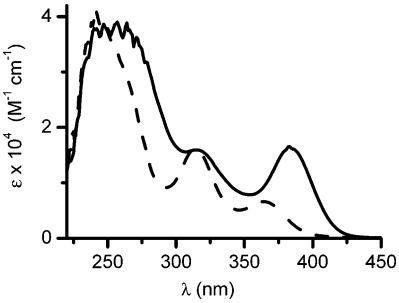

Figure 6. Electronic absorption spectra of **3** (—) and **5** (- - -) in dichloromethane solution at room temperature.

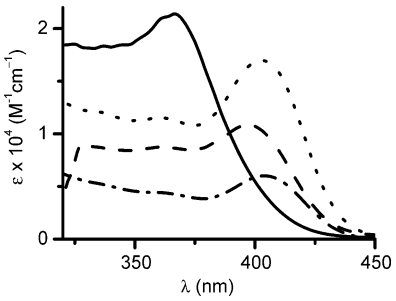

Figure 7. Low-energy absorption bands of the UV−vis spectra of complex **9** in acetonitrile (—), acetone (- - -), dichloromethane (···) and toluene (· − ·).

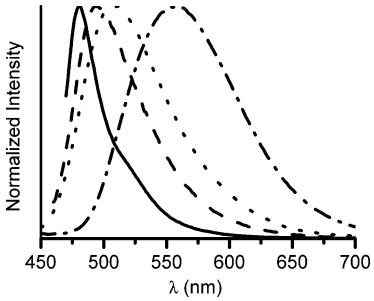

Figure 8. Emission spectra of the PtAg complexes **1** (—), **3** (- - -), **4** (···), and **5** (· − ·) in the solid state at room temperature.

> 300 nm. They also exhibit moderate solution luminescence in degassed dichloromethane at 298 K. The solid-state lifetime at 298 K is in the range of microseconds, revealing that the emission is most likely associated with a spin-forbidden triplet parentage. Vibronic-structured emission bands with vibrational progressional spacings of 1840−2040 cm^{-1} are observed at 77 K in some cases, which are typical for the ν(C≡C) stretching modes of the acetylides in the ground states. The appearance of vibronic progressions suggests the involvement of the acetylides in the excited states.

For the PtM heterobinuclear complexes, the emission energy of the PtM heterobinuclear complexes in the solid state or in frozen glasses at 77 K follows a trend with **1** > **3** > **4** > **5** (Figure 8) for the PtAg complexes and **6** > **8** > **9** > **10** for the PtCu complexes, which is in line with the electron-donating ability of the acetylides (C_6H_5 < $C_6H_4CH_3$-4 < $C_6H_4OCH_3$-4 < Bu^t). Therefore, it is likely that the emission is derived from alkynyl-to-cluster [RC≡C → PtM)] LMMCT triplet states in view of the short $Pt^{II}-M^{I}$ contacts.[13c,14a]

The PtAg complexes in degassed dichloromethane at 298 K display moderate emission at ca. 410−440 nm and a shoulder at ca. 525−550 nm with lifetimes in the ranges of nanoseconds and microseconds, respectively, revealing a dual emission nature. The higher energy (410−440 nm) emission is fluorescent in nature, whereas the emission shoulder at ca. 525−550 nm is probably associated with phosphorescence. In the degassed dichloromethane solutions at 298 K, however, the PtCu complexes only show the high-energy emission at ca. 415−455 nm with the nanosecond range of lifetimes.

The $PtCu_2$ heterotrinuclear complexes $[PtCu_2(dppm)_2(C{\equiv}CR)_2(CH_3CN)_2]^{2+}$ (R = C_6H_5 (**7**), $SiMe_3$ (**12**)) exhibit intense luminescence, whether in fluid solutions or in the solid state, with excitation at λ_{ex} > 350 nm. A remarkable red shift of the emission energy is observed on going from the complex **7** (R = C_6H_5) to **12** (R = $SiMe_3$), whether in the solid state or in the solutions, which is in line with the electron-donating ability of C_6H_5 < $SiMe_3$ in the acetylide ligands. Thus, the emissive origin of the $PtCu_2$ trinuclear complexes is likely associated with a ligand-to-cluster [RC≡C→$PtCu_2$)] charge-transfer transition, as suggested for the PtM binuclear complexes.

Excitation of the heteropentanuclear complex **13** with λ_{ex} > 350 nm affords intense emission in the solid state (λ_{em} = 576 nm at 298 K and λ_{em} = 567 nm at 77 K) and in frozen glass (λ_{em} = 543 nm) at 77 K. The emission energy is close to that of the $PtAg_2$ heterotrinuclear complex **2** but shows a significant red shift compared with that of the PtAg heterobinuclear complexes. It appears that formation of the pentanuclear cluster structures is favorable to reduce the energy gap between the HOMO and LUMO orbitals by increasing the contribution from the metal-centered emission. Compound **13** also displays moderate solution emission at ca. 437 nm with the lifetime τ_{em} = 3.2 ns in dichloromethane at 298 K, which is close to those found in the heterobinuclear PtAg complexes, indicative of their similar origin.

Conclusions

A series of PtM, PtM_2, and Pt_2Ag_3 heteronuclear alkynyl complexes were prepared by reaction of $[Pt(C{\equiv}CR)_4]^{2-}$ with 1 or 2 equiv of $[M_2(dppm)_2]^{2+}$ (M = Cu, Ag, Au). Formation of complexes with different nuclearities is correlated with the solvents and solution concentrations. The structural characterization of these $Pt^{II}-M^{I}$ heteronuclear complexes with different topologies was accomplished. These complexes emit strongly in the microsecond range of lifetimes in the solid state. They also exhibit moderate luminescence in the degassed solutions. In terms of the variation trend in the emission energy for the complexes containing various R substituents with different electronic effects, the emissive states are tentatively ascribed to involve substantial alkynyl-to-cluster [RC≡C→PtM] LMMCT transitions.

Acknowledgment. This work was supported by the NSFC (Grant Nos. 20273074, 20490210, and 90401005), the NSF of Fujian Province (Grant Nos. E0420002 and E0310029), the fund from the Chinese Academy of Sciences, and the National Basic Research Program (Grant No. 001CB108906) from the Ministry of Sciences and Technology of China.

Supporting Information Available: X-ray crystallographic files in CIF format for the structure determination of compounds **1** and **5**−**13**. This material is available free of charge via the Internet at http://pubs.acs.org.

OM050620E